



A Review of Energy and Exergy Analyses of a Roughened Solar Air Heater

Nguyen Minh Phu^{1,2,*}, Nguyen Thanh Luan^{1,2,3}

¹ Faculty of Mechanical Engineering, Ho Chi Minh City University of Technology (HCMUT), Ho Chi Minh City, Vietnam

² Vietnam National University, Ho Chi Minh City, Vietnam

³ Faculty of Vehicle and Energy Engineering, Ho Chi Minh City University of Technology and Education (HCMUTE), Ho Chi Minh City, Vietnam

ARTICLE INFO

Article history:

Received 23 June 2020

Received in revised form 11 September 2020

Accepted 12 September 2020

Available online 13 November 2020

ABSTRACT

In this paper, energy and exergy analyses of eleven roughness elements in solar air heater ducts were reviewed. Various roughness geometries, such as ribs, twisted tap, baffles, and metal waste, were surveyed for their effects on heat transfer and friction when the air flow passed over the absorber plate. The evaluation criteria for roughness elements on the absorber plate, including the thermohydraulic performance parameters, thermal efficiency, effective efficiency, and exergy efficiency, were presented and compared. The results showed that protruding ribs in an arc shape resulted in the largest Nusselt number. The ribs exhibited the highest thermohydraulic performance parameters at a Reynolds number greater than 5000. Jet impingement with arc-shaped ribs and roughness elements in metal waste were found to result in the smallest exergy efficiencies. The largest effective and exergy efficiencies were 70% and 1.9%, respectively. The thermohydraulic performance parameter varied from 0.5 to 2.0. This review paper aims to provide information about roughness geometries by investigating both the first and second laws of thermodynamics and the figure of merits to describe artificial roughness in a solar air heater.

Keywords:

Thermohydraulic; Solar air heater;
Energy analysis; Exergy analysis

1. Introduction

Energy shortages and environmental pollution are pressing problems in modern society. One of the reasons for these problems is the burning of fossil fuels to operate thermal power plants, which emit large amounts of carbon dioxide [1,2]. In addition, CFC and HCFC refrigerants in air conditioners cause greenhouse effects and global warming [3,4]. Using renewable energy as an alternative to fossil fuels has received much attention in recent decades. Solar energy is attracting increasing attention because of its large amount and its presence throughout the planet.

* Corresponding author.

E-mail address: nmpu@hcmut.edu.vn

<https://doi.org/10.37934/arfmts.77.2.160175>

The solar air heater (SAH) is perhaps the simplest and most reliable solar thermal energy converter. The device converts solar thermal energy into a hot air stream that can be used for heating or drying [5]. However, due to the nondominant thermophysical properties of the air, the efficiency of the air collector is not high. Therefore, obstacles are often placed into SAH ducts to remove the laminar sub-layer of air closest to the absorber surface and to mix the primary and secondary flows along the heater length. The shape of the obstacles in a SAH is very diverse. They can be ribs, fins or baffles, which are commonly known as roughened SAH. The literature has revealed several evaluation criteria for roughened SAH. Among these criteria, the thermohydraulic performance parameter is used to estimate the heat transfer enhancement due to the pressure loss penalty, and the exergy efficiency is used to qualify the loss components due to irreversibility. There have been many review articles on energy or exergy analysis of roughness in SAH. To the best of our knowledge, a survey of the roughness geometries of solar air heaters according to both the first and second laws of thermodynamics has not been conducted. Such a survey is essential because it demonstrates that the roughness geometry has not yet been examined sufficiently. In this review, eleven state-of-the-art roughness geometries that have been studied in terms of both energy and exergy were analysed and evaluated. The article summarizes and provides information on each type of roughness and efforts by researchers to clarify both the energy and exergy points of view. Therefore, the main objective of the present work is to analyse and observe the different roughness shapes of SAH to qualify high performance and facilitate practical application. The procedure used for roughness studies in previous works involved the calculation of the Nusselt number and the friction factor correlations. The equations were then used to evaluate the thermohydraulic performance, thermal efficiency, effective efficiency, entropy generation, and exergy efficiency.

2. Roughness Geometries in Terms of Both Energy and Exergy

Figure 1 contains a schematic diagram of an SAH. Solar energy passes through the glass cover into the absorber plate. Air blows through the clearance between the glass cover and the absorber plate to acquire thermal energy from the plate. Roughness elements are attached to the absorber surface to enhance heat exchange. Table 1 summarizes the roughness elements that have been studied to assess both the thermohydraulic and exergy performance. The Nusselt number (Nu) represents the heat exchange, and the friction factor (f) denotes the pressure loss of the air flowing across the roughened channel. The formulation of the Nu and f equations uses either experimental or numerical (CFD) approaches. Both approaches were performed as per ASHRAE standard 93-97. Normally, the Nu and f equations are functions of the Reynolds number (Re), relative roughness pitch (P/e), relative roughness height (e/D_h), angle of attack (α) and other geometric parameters. It is evident that the Nu and f values of the roughened duct are larger than those of the smooth duct. The exergy analysis was used to identify the exergy loss components with the greatest irreversibility and exergy efficiency, which are shown in Table 1. The exergy performance of SAH is very low due to the large exergy loss resulting from the large difference between the sun temperature and the absorber plate temperature. To compare the heat transfer enhancement and the pressure loss penalty due to the roughness, investigators often use the following well-known formulas for smooth ducts.

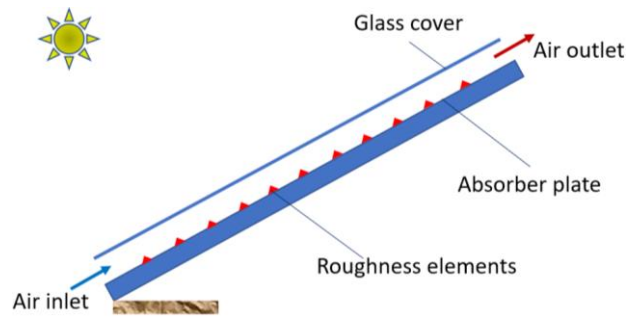


Fig. 1. Solar air heater

Dittus-Boelter correlation for the Nusselt number

$$Nu_{smooth} = 0.023Pr^{0.4} Re^{0.8} \quad (1)$$

Blasius correlation for the friction factor

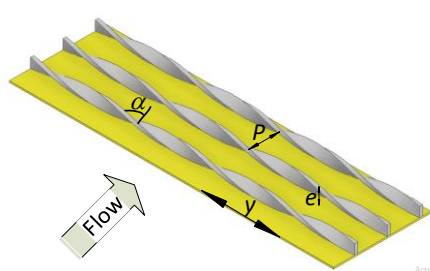
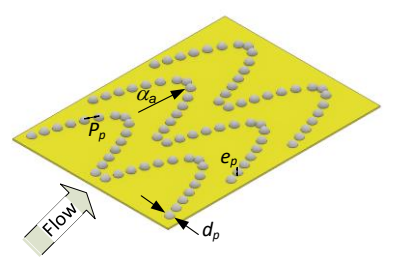
$$f_{smooth} = 0.079Re^{-0.25} \quad (2)$$

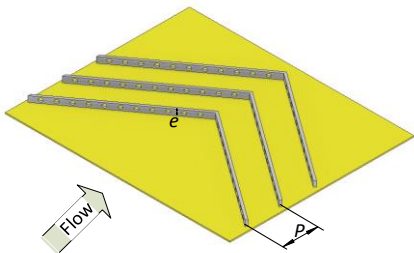
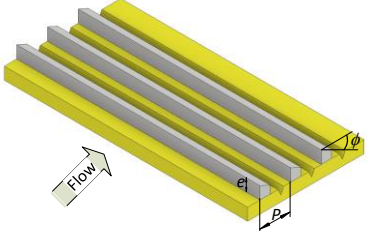
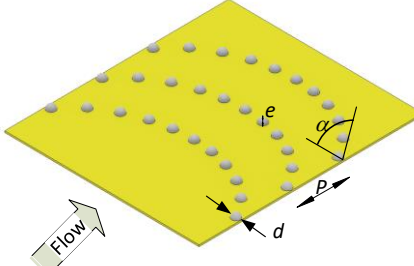
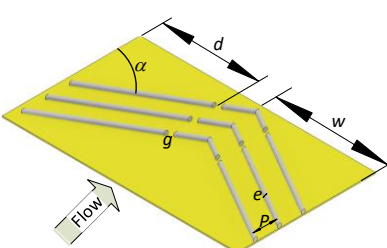
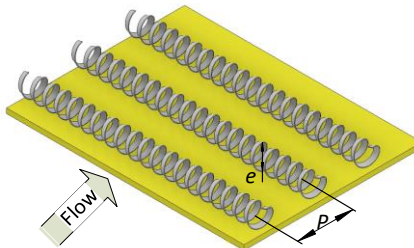
To evaluate the difference between the gain due to heat transfer and the loss in pressure, a thermohydraulic performance parameter is used. This parameter is defined as follows

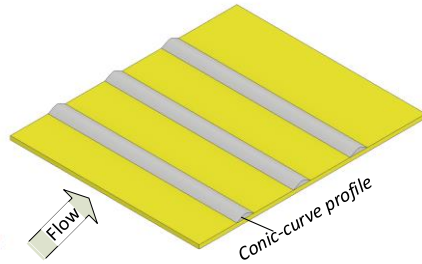
$$\eta = \frac{Nu / Nu_{smooth}}{(f / f_{smooth})^{1/3}} \quad (3)$$

Table 1

Roughness shapes in SAH duct studied both thermohydraulic and exergy analyses

No.	Roughness shape	Researchers and remarks in thermohydraulic research	Researchers and remarks in exergy research
1.		Kumar and Layek [6] Nusselt number and friction factor 2.46 and 1.78 times higher than those of a smooth plate $Nu = 3 \times 10^{-10} Re^{1.043} (y/e)^{-0.17} (P/e)^{15.75} (\alpha/90)^{-0.84} \exp(-3.75(\ln(P/e))^2) \exp(-0.85(\ln(\alpha/90))^2)$	Kumar and Layek [7] Exergetic efficiency 1.81 times higher than that of a smooth plate
2.		Nadda <i>et al.</i> , [8] Largest thermohydraulic performance parameter of 3.64 $Nu = 0.0476Re^{1.0119} (W_A/W_{AP})^{0.4228} \exp(0.0529(\ln(W_A/W_{AP}))^2) (e_r/d_r)^{-0.133} \exp(-0.228(\ln(e_r/D_r))^2) (P_r/e_r)^{-0.1455} \exp(-0.3069(\ln(P_{p,r}))^2) (\alpha_a/55)^{-0.7522} \exp(-1.4876 \cdot (\ln(\alpha_a/55))^2)$ $f = 15.601Re^{-0.1434} (W_A/W_{AP})^{0.2569} \exp(0.1205(\ln(W_A/W_{AP}))^2) (e_r/d_r)^{-0.1708} \exp(-0.3957(\ln(e_r/d_r))^2) (P_r/e_r)^{-0.2777} \exp(-0.5793 \cdot (\ln(P_r/e_r))^2) (\alpha_a/55)^{-0.9011} \exp(-1.7618(\ln(\alpha_a/55))^2)$	Matheswaran <i>et al.</i> , [9] Maximum exergetic efficiency of 10.5%

3. V-down perforated baffles		<p>Chamoli and Thakur [10,11] Highest increase in heat transfer of 2.2 times and friction factor of 5.2 times</p> $Nu = 0.0296Re^{0.7848} (P/e)^{0.3007} (e/H)^{-0.6774} \beta^{-0.3571} \exp(-0.2548 \ln(P/e)^2) \exp(-0.4406 \ln(e/H)^2) \exp(-0.0863 \ln(\beta)^2)$ $f = 0.632Re^{-0.18} (P/e)^{-0.16} (e/H)^{1.05} \beta^{-0.13}$	<p>Chamoli and Thakur [12] Highest increase in exergetic efficiency of 76%</p>
4. Chamfered rib with groove		<p>Karwa <i>et al.</i>, [13] 2-fold increase in Stanton number and 3-fold increase in friction factor</p> $Nu = 0.0028Re^{0.93} (e/D_h)^{0.528} (P/e)^{2.17} (g/P)^{-1.054} \phi^{0.77} \exp(-0.138(\ln(\phi))^2) \exp(-0.57(\ln(P/e))^2) \exp(-0.649(\ln(g/P))^2)$ $f = 0.00276Re^{-0.1279} (e/D_h)^{0.3632} (P/e)^{4.255} (g/P)^{-0.976} \exp(0.00575\phi) \exp(-1.066(\ln(P/e))^2) \exp(-0.583(\ln(g/P))^2)$	<p>Layek <i>et al.</i>, [14] Larger relative roughness height, smaller entropy generation</p>
5. Protruded ribs in arc shape		<p>Yadav and Kaushal [15] Maximum increase in Nusselt number of 2.89 times and friction factor of 2.93 times</p> $Nu = 0.154Re^{1.107} (P/e)^{-0.38} (e/D_h)^{0.521} (\alpha/60)^{-0.213} \exp(-2.023(\ln(\alpha/60))^2)$ $f = 7.207Re^{-0.56} (P/e)^{-0.18} (e/D_h)^{0.176} (\alpha/60)^{0.038} \exp(-1.412(\ln(\alpha/60))^2)$	<p>Yadav and Kaushal [16] Maximum exergetic efficiency of 2.25%</p>
6. Discrete V-down ribs		<p>Singh <i>et al.</i>, [17] Maximum increase in Nusselt number of 3.04 times and friction factor of 3.11 times</p> $Nu = 2.36 \times 10^{-3} Re^{0.9} (P/e)^{3.5} (\alpha/60)^{-0.023} (d/w)^{-0.043} (g/e)^{-0.014} (e/D_h)^{0.47} \exp(-0.84(\ln(p/e))^2) \exp(-0.72(\ln(\alpha/60))^2) \exp(-0.05(\ln(d/w))^2) \exp(-0.15(\ln(g/e))^2)$ $f = 4.13 \times 10^{-2} Re^{-0.126} (P/e)^{2.74} (\alpha/60)^{-0.034} (d/w)^{-0.058} (g/e)^{0.031} (e/D_h)^{0.7} \exp(-0.685(\ln(p/e))^2) \exp(-0.93(\ln(\alpha/60))^2) \exp(-0.058(\ln(d/w))^2) \exp(-0.21(\ln(g/e))^2)$	<p>Singh <i>et al.</i>, [18] Maximum exergetic efficiency of 2%</p>
7. Helically coiled metal waste		<p>Phu <i>et al.</i>, [19] The optimum relative roughness height is 0.35 to obtain the highest thermo-hydraulic performance parameter</p> $Nu = 0.0753297Re^{0.901077} (e/D_h)^{0.169444} (p/e)^{-0.668855}$ $f = 16.9194Re^{-0.358125} (e/D_h)^{0.527405} (p/e)^{-0.875926}$	<p>Phu <i>et al.</i>, [20] The largest exergy efficiency of 2.7% is achieved at an absorber plate aspect ratio of 3</p>
8. Conic-curve profile ribs	<p>Ngo and Phu [21] Hyperbolic ribs ($K = -4$) obtained the highest thermohydraulic performance For conic constant, $K < 0$</p>	<p>Phu and Hap [22] The largest exergy efficiency was 1.53% at a</p>	



9. V-ribbed triangular duct

$$Nu = 0.0152703Re^{0.898047} abs(K)^{0.023995}$$

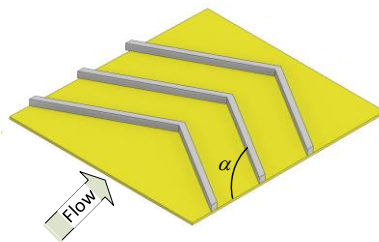
$$f = 0.0252542Re^{-0.0407643882} abs(K)^{-0.0182465}$$

For conic constant, K=0

$$Nu = 0.0171061297Re^{0.878853933}$$

$$f = 0.0243164038Re^{-0.0345346707}$$

Reynolds number of 2800



Kottayat *et al.*, [23]

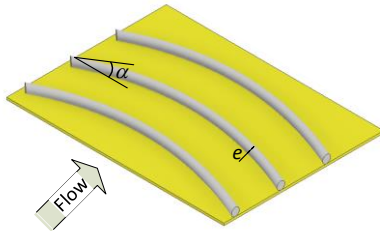
The highest thermohydraulic performance of 2.01 at Reynolds number of 7500

$$Nu = 1.49 \times 10^{-6} Re^{0.77} \alpha^{5.7} \exp\left(-0.76\left(\ln(\alpha)^2\right)\right)$$

$$f = Re^{-0.101909381} \left(\begin{array}{l} 0.31821672 - 0.0217751549\alpha + 0.000587209098\alpha^2 \\ -0.00000651943045\alpha^3 + 2.54340956 \times 10^{-8}\alpha^4 \end{array} \right)$$

Kottayat *et al.*, [23]
 Enhancement in exergy efficiency of 23% is drawn

10. Arc-shaped wire



Saini and Saini [24]

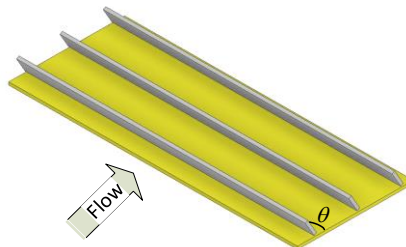
The maximum enhancement in Nusselt number was obtained as 3.80 times and the augmentation in friction factor was 1.75 times

$$Nu = 0.001047Re^{1.3186} (e/D_h)^{0.3772} (\alpha/90)^{-0.1198}$$

$$f = 0.14408Re^{-0.17103} (e/D_h)^{0.1765} (\alpha/90)^{0.1185}$$

Sahu and Prasad [25]
 Enhancement in exergy efficiency of 56% was earned

11. Inclined baffles



Phila *et al.*, [26], Luan and Phu [27]

The highest thermohydraulic performance of 1.11 at Reynolds number of 9000

$$Nu = Re^{0.70124712} \left(\begin{array}{l} 0.0609074696 - 0.000313948974\theta + 0.0000491085268\theta^2 \\ -0.00000124195437\theta^3 + 1.34125344 \times 10^{-8}\theta^4 \\ -6.66643132 \times 10^{-11}\theta^5 + 1.24227417 \times 10^{-13}\theta^6 \end{array} \right)$$

$$f = 0.25Re^{-0.272516828} \left(\begin{array}{l} 1.01982341 - 0.00035175506\theta + 0.00035831535\theta^2 \\ -0.0000108633445\theta^3 + 1.31604401 \times 10^{-7}\theta^4 \\ -7.07752718 \times 10^{-10}\theta^5 + 1.39342043 \times 10^{-12}\theta^6 \end{array} \right)$$

Luan and Phu [27]
 The highest exergy efficiency was 0.7% at a Reynolds number of 1500

For the purpose of comparing the Nu and f values of the roughness types and those of the smooth ducts, Figure 2 and Figure 3 show the Nu and f values according to the Re number. Protruding ribs in an arc shape and a chamfered rib with a groove greatly enhance the heat transfer. Heat transfer enhancement by protruding ribs was obtained due to main flow impingement, vortex formation on both sides of the protrusion and flow separation [15,28]. The magnitude of the Nu value of these obstacles is 3 times greater than that of the smooth duct. Roughness methods resulting in moderate heat transfer improvement include jet impingement with arc-shaped ribs, inclined baffles, V-down perforated baffles and metal waste (Figure 2).

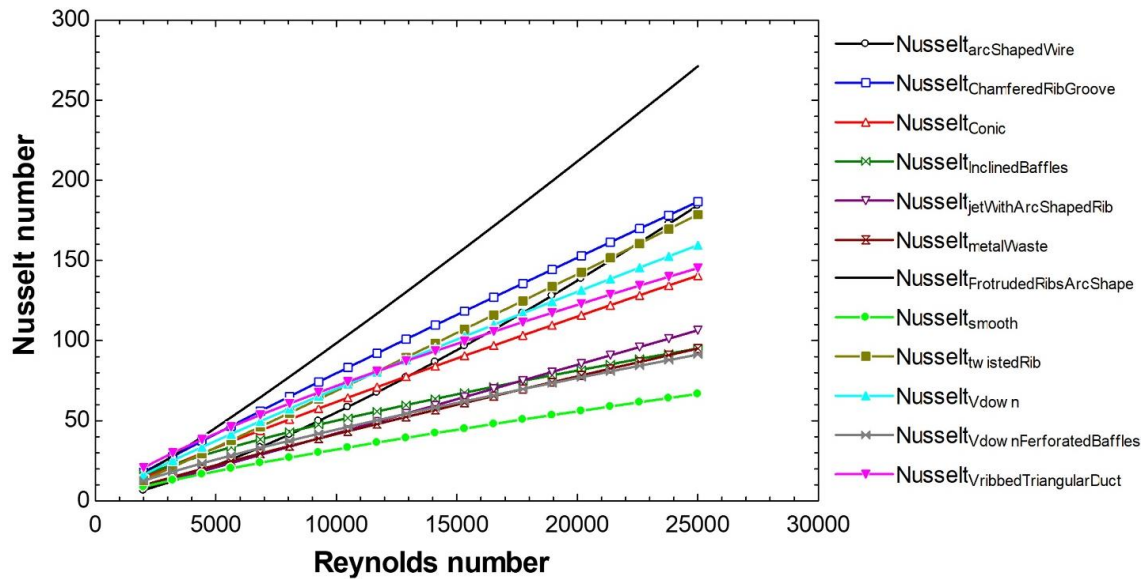


Fig. 2. Nusselt numbers for the smooth and roughened solar air heater ducts

V-down perforated baffles on the absorber surface also have a large friction factor, as shown in Figure 3. This is probably due to the small relative roughness pitch (P/e) (1 to 4). The optimal relative roughness pitch is approximately 10, as reported in the literature. Geometries with almost identical friction factors include the V-ribbed triangular duct, V-down rib, and conic rib.

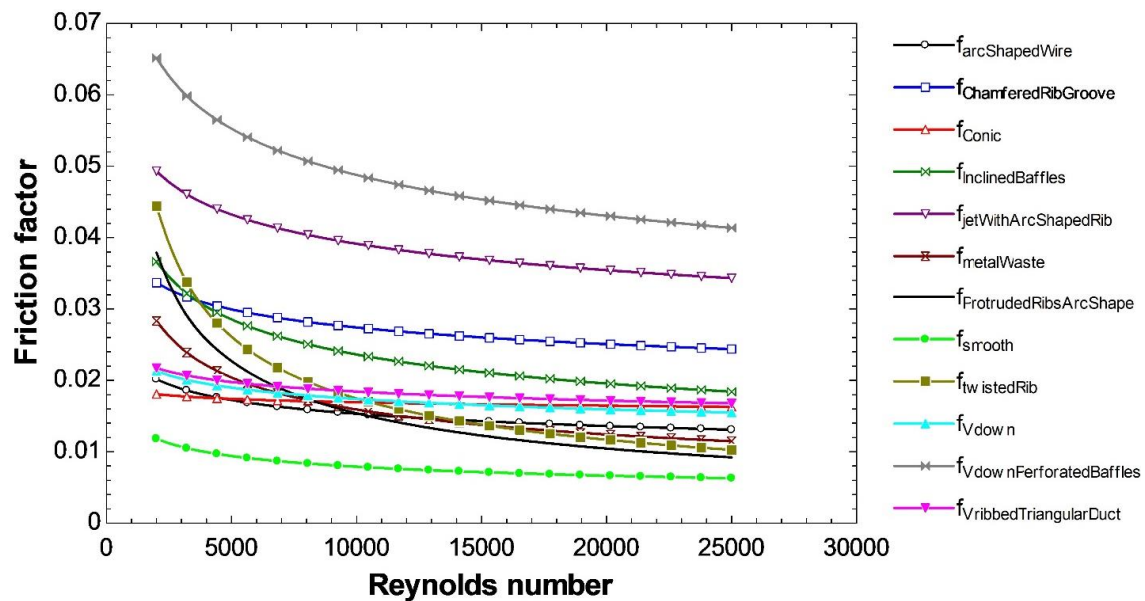


Fig. 3. Friction factors for the smooth and roughened solar air heater ducts

The trends of the Nu value and f factor reflect the thermohydraulic performance parameters, as shown in Figure 4. It can be seen that V-down perforated baffles result in the lowest values and protruded ribs in an arc shape result in the highest values. Most geometries result in values for this parameter greater than unity except V-down perforated baffles and jet impingement with arc-shaped ribs. The twisted rib results in the highest parameter values when the air flow is in turbulent mode ($Re > 10000$). This is due to an increase in flow impingement and jet formation due to the twisted rib [6].

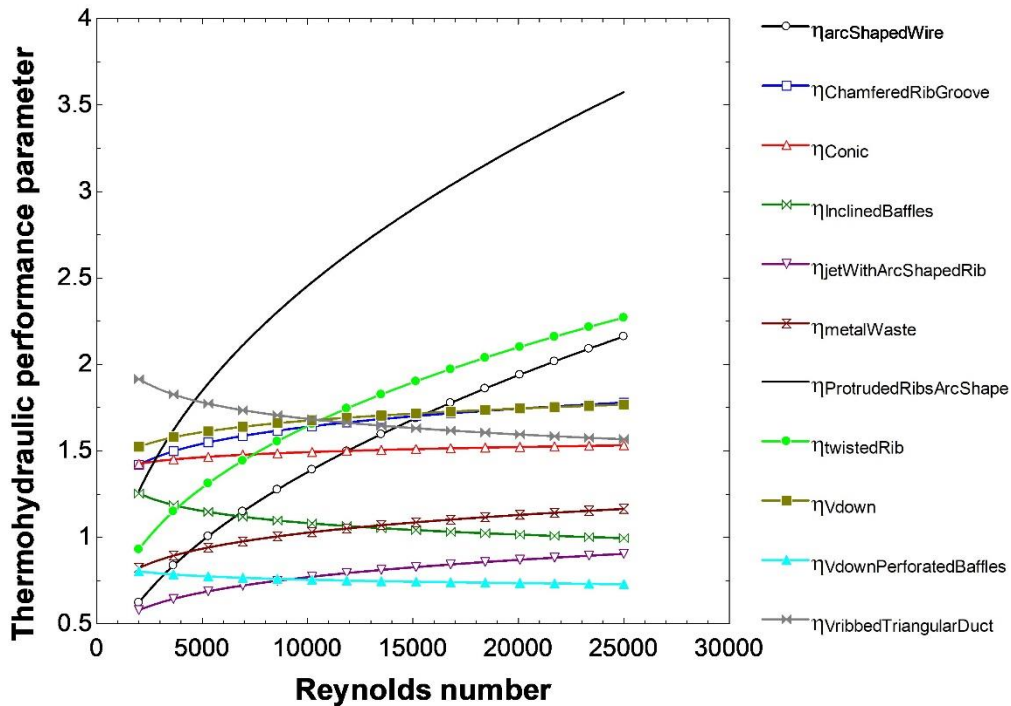


Fig. 4. Thermohydraulic performance of roughened solar air heater ducts

3. Efficiencies of Roughened Solar Air Heater

3.1 Thermal Efficiency

The equations below present a model for calculating SAH's performance such as thermal efficiency, effective efficiency and exergy efficiency. This model has been adopted by many researchers in the exergy study of SAH [7,9,12,14,16,18,20,22,23,25,27]. The useful heat gain of air flow acquired from solar radiation can be calculated by the following equations

$$\dot{Q}_u = A_c [I(\tau\alpha) - U_L(T_{ap} - T_a)] \tag{4}$$

$$\dot{Q}_u = \dot{m}c_p(T_o - T_i) = \dot{m}c_p\Delta T \tag{5}$$

$$\dot{Q}_u = A_c F_R [I(\tau\alpha) - U_L(T_o - T_i)] \tag{6}$$

where A_c is the absorber plate area, I is solar radiation, $\tau\alpha$ is the effective transmittance-absorptance product, \dot{m} is the mass flow rate of air, c_p is the specific heat of air at a constant pressure, F_R is the heat removal factor of the solar collector, U_L is the total loss coefficient, and T_{ap} , T_a , T_i , and T_o are the mean absorber plate temperature, ambient temperature, air inlet temperature, and air outlet temperature, respectively. The total loss coefficient from the solar collector to the surroundings can be estimated as follows

$$U_L = U_t + U_b + U_e \tag{7}$$

where U_t , U_b , and U_e are the loss coefficients at the top, bottom, and edge sides of the solar air heater, respectively. The top convective heat transfer coefficient is determined as follows

$$U_t = \left(\frac{N}{(C_t / T_{ap}) \left(\frac{T_{ap} - T_a}{N + f_t} \right)^e + 1 / h_w} \right)^{-1} + \sigma (T_{ap} + T_a) \frac{T_{ap}^2 + T_a^2}{\frac{1}{\varepsilon_{ap} + 0.00591 N h_w} + \frac{2N + f_t - 1 + 0.133 \varepsilon_{ap} - N}{\varepsilon_g}} \quad (8)$$

where,

$$C_t = 520(1 - 0.000051\beta_t^2)$$

$$e = 0.43(1 - 100 / T_{ap})$$

$$f_t = (1 + 0.089h_w - 0.1166h_w\varepsilon_{ap})(1 + 0.07866N)$$

in which β_t , ε_{ap} , ε_g , and N are the tilt angle of the heater, emissivity of the absorber plate, emissivity of the glass cover, and number of glass covers, respectively.

The convective heat transfer due to wind (h_w) is calculated by the following equation, which was reported by McAdams and considers the combined effects of convection and radiation

$$h_w = 5.7 + 3.8V_w \quad (9)$$

where V_w is the wind velocity.

Heat loss due to conduction of insulation at the back side of the heater can be estimated by the Fourier equation: $A_c(k_i/L_i)(T_p - T_b)$, where k_i , L_i , and T_b are the thermal conductivity, insulation thickness, and back temperature, respectively. Therefore, the bottom loss coefficient can be determined as follows

$$U_b = k_i / L_i \quad (10)$$

Because the edge losses of the collector are small, a one-dimensional heat flow around the perimeter of a collector of area LW and thickness Z is assumed. The losses through the edge are referenced to the collector area. Therefore, the edge loss coefficient is defined as follows

$$U_e = \frac{(L+W)Zk_i}{LWL_i} \quad (11)$$

where k_i and L_i are the thermal conductivity and thickness of the insulation, respectively, and L , W , and Z are the length, width, and depth of the solar air heater duct, respectively.

The heat removal factor is calculated as follows

$$F_R = \frac{\dot{m}c_p}{U_L A_c} \left[\exp \left(U_L A_c \frac{F_p}{\dot{m}c_p} \right) - 1 \right] \quad (12)$$

where F_p is the collector efficiency factor. This factor is expressed as follows

$$F_p = \frac{h}{h + U_L} \quad (13)$$

where h is the convective heat transfer coefficient between the air and absorber plate.

$$h = Nu \frac{k}{D_h} \quad (14)$$

The Nusselt number (Nu) is calculated from the equations listed in Table 1. The hydraulic diameter of the passage (D_h) and the Reynolds number (Re) are stated as follows

$$D_h = \frac{4WZ}{2(W + Z)} \quad (15)$$

$$Re = \frac{\dot{m}D_h}{\mu WZ} \quad (16)$$

The thermal efficiency is defined as the ratio of the useful heat gain of the air flow to the solar radiation on the surface of the SAH

$$\eta_t = \frac{\dot{Q}_u}{IA_c} \quad (17)$$

3.2 Effective Efficiency

The first law efficiency merely considers the useful heat received compared to the solar energy to the SAH surface. However, the energy required to transport the working fluid through the SAH has not been taken into account. Hence, the effective efficiency is defined as follows

$$\eta_{Eff} = \frac{\dot{Q}_u}{IA_c} - \frac{P_m}{IA_c C_j} \quad (18)$$

where C_j is the thermal energy conversion factor, which the literature recommends to be set at 0.2. The pumping power is calculated as follows

$$P_m = \frac{\dot{m}\Delta p}{\rho} \quad (19)$$

where ρ is the density of air and Δp is the pressure difference in the air flow. The air pressure difference is expressed as follows

$$\Delta p = 4f\rho \frac{LV^2}{2D_h} \quad (20)$$

where the mean air velocity inside the SAH duct (V) is computed as follows

$$V = \frac{\dot{m}}{\rho WZ} \quad (21)$$

The friction factor (f) can be found from Table 1 for different types of roughness.

3.3 Exergy Efficiency

Exergy analysis is a tool for finding components in a heat system that have great exergy destruction and high irreversibility. In this analysis, a solution is sought to maximize exergy efficiency or minimize entropy generation. For an SAH, the following exergy loss components are included

- i. Optical exergy losses

$$EX_{loss,opt} = IA_c (1 - \tau\alpha) \left[1 - (4/3)(T_a / T_{sun}) + (1/3)(T_a / T_{sun})^4 \right] \quad (22)$$

where T_{sun} is the sun temperature.

- ii. Exergy losses by convection and radiation heat transfer from the absorber plate to the environment

$$EX_{loss,Q_{loss}} = U_L A_c (T_{ap} - T_a) (1 - T_a / T_{ap}) \quad (23)$$

- iii. Exergy losses by absorption of radiation by the absorber plate

$$EX_{loss,T_{ap},T_{sun}} = IA_c \tau\alpha \left[1 - (4/3)(T_a / T_{sun}) + (1/3)(T_a / T_{sun})^4 - (1 - T_a / T_{ap}) \right] \quad (24)$$

- iv. Exergy losses by heat transfer to the working air

$$EX_{loss,T_{ap},T_f} = IA_c \eta_I T_a (1 / T_f - 1 / T_{ap}) \quad (25)$$

where T_f is the mean temperature of the working air, $T_f = 0.5(T_i + T_o)$.

- v. Frictional exergy losses of the working air

$$EX_{loss,friction} = \frac{\dot{m}\Delta p T_a}{\rho T_f} \quad (26)$$

The first two kinds of exergy losses are external losses. The remaining kinds are known as internal losses. The total exergy losses are determined by summing the abovementioned exergy losses

$$\sum EX_{loss} = EX_{loss,opt} + EX_{loss,Q_{loss}} + EX_{loss,T_{ap},T_{sun}} + EX_{loss,T_{ap},T_f} + EX_{loss,friction} \quad (27)$$

The input exergy of the SAH is constituted by the air inflow and solar radiation source as follows:

$$\sum EX_{inlet} = IA_c \left[1 - (4/3)(T_a / T_{sun}) + (1/3)(T_a / T_{sun})^4 \right] \quad (28)$$

The exergy efficiency can be calculated by summing the total exergy losses and input exergy as follows [9]

$$\eta_{II} = 1 - \sum EX_{loss} / \sum EX_{inlet} \quad (29)$$

Table 2 presents the inputs into the mathematical model above to calculate and compare yields for different types of roughness. These parameters are widely used in the exergy performance studies of SAH.

Table 2
 Values of operating and design parameters

Parameter	Value
Air inlet temperature (T_i)	300 K
Ambient temperature (T_a)	300 K
Depth of the collector (Z)	0.025 m
Effective transmittance-absorptance product ($\tau\alpha$)	0.8
Emissivity of glass cover (ϵ_g)	0.88
Emissivity of the absorber plate (ϵ_{ap})	0.9
Length of the collector (L)	1.5 m
Number of glass covers (N)	1
Reynolds number (Re)	2000 to 25,000
Solar radiation (I)	1000 W m ⁻²
Sun temperature (T_{sun})	5800 K
Thermal conductivity of the insulation (k_i)	0.037 W m ⁻¹ K ⁻¹
Thickness of the insulation (L_i)	20 mm
Width of the collector (W)	1 m
Wind velocity (V_w)	1 m/s
Relative roughness pitch (P/e)	8
Relative roughness height (e/D_h)	0.03
Angle of attack (α)	60°

The effect of the temperature rise on the thermal efficiency is presented in Figure 5. It should be noted that the parameter is inversely proportional to the Reynolds number for a given solar radiation I . The temperature rise (ΔT) is the air temperature difference, which was defined in Eq. (5). When the parameter increases, the Re number decreases, leading to a decrease in the Nusselt number. In other words, the useful heat gain decreases with an increase in the temperature rise parameter. From the analysis of the heat transfer rate described in the previous section, it can be seen that protruding ribs in an arc shape and jet impingement with arc-shaped ribs result in the largest and smallest thermal

efficiency, respectively. The maximum effective efficiency for certain temperature rises values and roughness geometries can be observed in Figure 6. This is because the increase in the parameter results in a trade-off between decreased heat transfer and decreased pressure loss. The highest effective efficiency was obtained at a parameter value of 0.006 K.m²/W. The largest value of 72% was obtained by using the protruded ribs in an arc-shape.

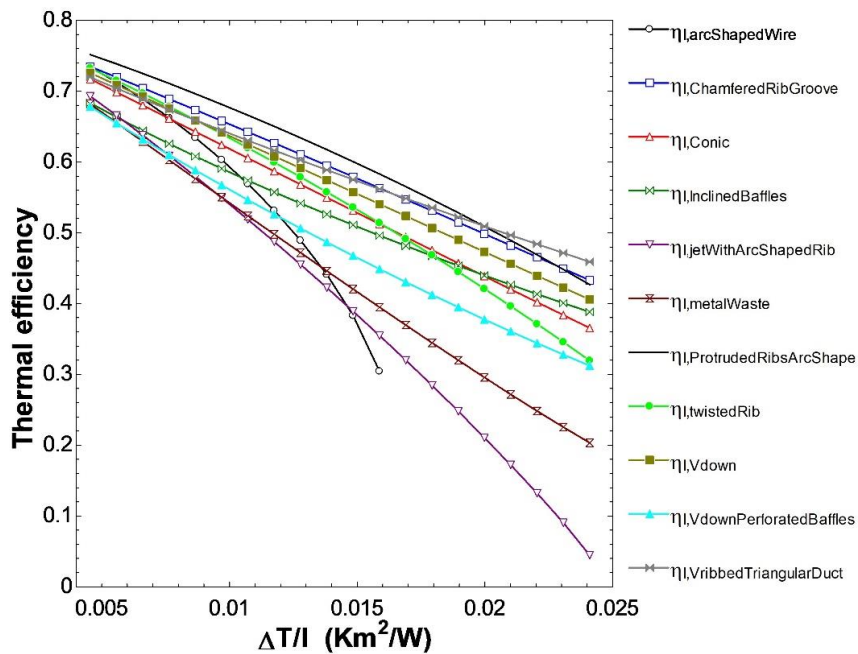


Fig. 5. Variation in the thermal efficiency with an increase in the temperature parameter

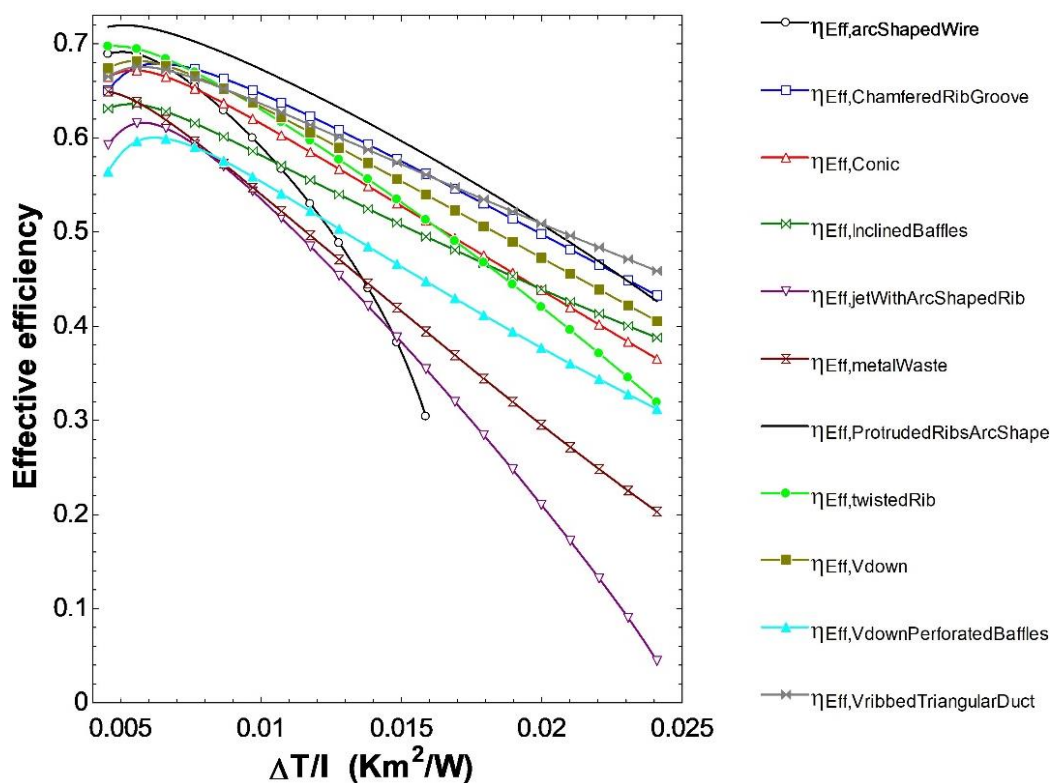


Fig. 6. Variation in the effective efficiency with the temperature rise parameter

The exergy efficiency as a function of the temperature rise parameter and roughness geometry is displayed in Figure 7. Generally, the efficiency was rather low (less than 2%) for all eleven of the considered roughness elements. This was mainly due to exergy losses caused by the absorption of radiation by the absorber plate ($EX_{loss, Tap, Tsun}$) and optics ($EX_{loss, opt}$) [29]. At very low temperature rise parameters, $EX_{loss, Tap, Tsun}$ was remarkably high. Therefore, the exergy efficiency became negative, as shown in Figure 7. The maximum exergy efficiency of a certain roughness element can also be seen, such as jet impingement with arc-shaped ribs, metal waste, twisted ribs, and arc-shaped wires. This is because increasing the parameter increases exergy losses by convection and radiation heat transfer ($EX_{loss, Qloss}$). These trends showed a minimum total exergy loss, as displayed in Figure 8. The roughness geometries with the highest and lowest exergy efficiencies can also be observed in Figure 7, which was inferred and commented on in the previous section.

Altfeld *et al.*, [30] pointed out that the exergy efficiency can be maximized by adjusting the temperature level of the collector or the duct geometry and flow velocity. Sahu and Prasad [25] found that a relative roughness height $e/D_h = 0.0422$, a relative roughness pitch $P/e = 10$, and a relative angle of attack $\alpha/90 = 0.3333$ yielded the maximum exergy efficiency for solar air heaters with arc-shaped wires. In particular, Ghritlahre *et al.*, [31,33,34] and Ghritlahre [32] recommended the use of the artificial neural network (ANN) technique to predict the energy and exergy performance of a SAH due to its high accuracy.

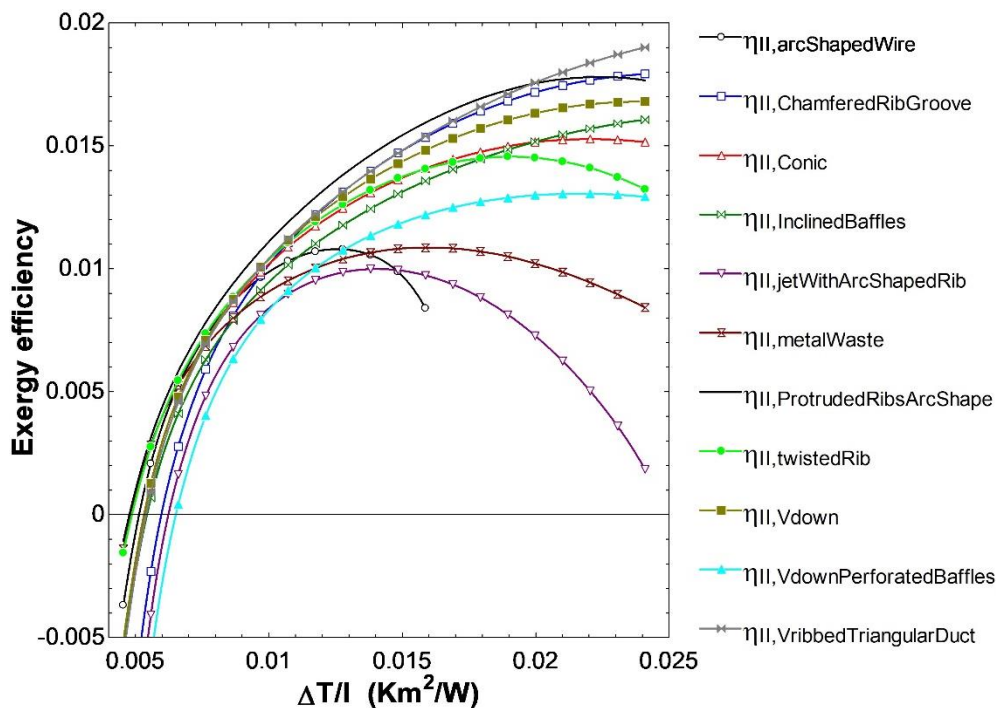


Fig. 7. Variation in the exergy efficiency with the temperature rise parameter

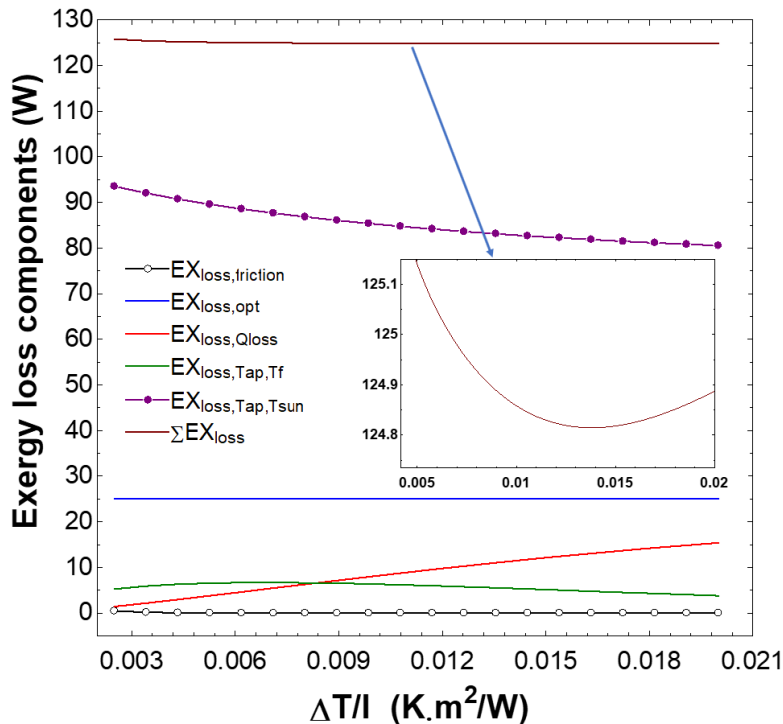


Fig. 8. Exergy loss components for inclined baffles with $\theta = 60^\circ$

4. Conclusions

The characteristics of thermohydraulics and the efficiencies of the roughness geometries of solar air heater ducts have been reported in this study. The Nusselt numbers, friction factors, thermohydraulic performance, thermal efficiency, effective efficiency, and exergy efficiency have been presented as functions of the Reynolds number and the temperature rise parameter. The findings of this review are as follows

- i. The highest effective efficiency can be obtained at a temperature rise parameter of 0.006 $\text{K.m}^2/\text{W}$.
- ii. High exergy efficiency can be obtained at a temperature rise parameter between 0.01 to 0.02 $\text{K.m}^2/\text{W}$ for jet impingement with arc-shaped ribs, metal waste, twisted ribs, and arc-shaped wires.
- iii. Protruded ribs in an arc shape have a high heat transfer ability and low-pressure loss. Therefore, these ribs have outstanding performance compared to the rest of the roughness elements.
- iv. The exergy efficiency is rather low (less than 2%) for all eleven considered roughness elements. An optimization procedure needs to be employed to maximize exergy performance.
- v. For artificial roughness elements that have not been subjected to exergy analysis, it is recommended to conduct follow-up studies to provide comprehensive information for the type of roughness.

References

- [1] Phu, Nguyen Minh, Pham Ba Thao, and Duong Cong Truyen. "Comparative Study and Optimization of CO₂ Capture and Storage in LNG-fired Power Plant." *Journal of Advanced Research in Fluid Mechanics and Thermal Sciences* 72, no. 2 (2020): 55-66.

- [2] Nguyen, Phu Minh. "Energy and exergy estimation for a combined cycle of solid CO₂ production and NH₃-H₂O single effect absorption chiller." *Science and Technology Development Journal* 19, no. 1 (2016): 61-69. <https://doi.org/10.32508/stdj.v19i1.611>
- [3] Tuyen, Vo, Nguyen Van Hap, and Nguyen Minh Phu. "Thermal-hydraulic characteristics and optimization of a liquid-to-suction triple-tube heat exchanger." *Case Studies in Thermal Engineering* (2020): 100635. <https://doi.org/10.1016/j.csite.2020.100635>
- [4] Nguyen, Minh Phu, and Geun-Sik Lee. "Characteristics of the water pressure drop considering heat transfer in the evaporator and condenser of a water chiller." *Transactions of the Korean Society of Mechanical Engineers B* 35, no. 12 (2011): 1293-1300. <https://doi.org/10.3795/KSME-B.2011.35.12.1293>
- [5] Nguyen, Minh Phu, Tu Thien Ngo, and Thanh Danh Le. "Experimental and numerical investigation of transport phenomena and kinetics for convective shrimp drying." *Case Studies in Thermal Engineering* 14 (2019): 100465. <https://doi.org/10.1016/j.csite.2019.100465>
- [6] Kumar, Anup, and Apurba Layek. "Nusselt number and friction factor correlation of solar air heater having twisted-rib roughness on absorber plate." *Renewable Energy* 130 (2019): 687-699. <https://doi.org/10.1016/j.renene.2018.06.076>
- [7] Kumar, Anup, and Apurba Layek. "Energetic and exergetic performance evaluation of solar air heater with twisted rib roughness on absorber plate." *Journal of Cleaner Production* 232 (2019): 617-628. <https://doi.org/10.1016/j.jclepro.2019.05.363>
- [8] Nadda, Rahul, Anil Kumar, and Rajesh Maithani. "Developing heat transfer and friction loss in an impingement jets solar air heater with multiple arc protrusion obstacles." *Solar Energy* 158 (2017): 117-131. <https://doi.org/10.1016/j.solener.2017.09.042>
- [9] Matheswaran, M. M., T. V. Arjunan, and D. Somasundaram. "Analytical investigation of exergetic performance on jet impingement solar air heater with multiple arc protrusion obstacles." *Journal of Thermal Analysis and Calorimetry* 137, no. 1 (2019): 253-266. <https://doi.org/10.1007/s10973-018-7926-z>
- [10] Chamoli, Sunil, and N. S. Thakur. "Heat transfer enhancement in solar air heater with V-shaped perforated baffles." *Journal of Renewable and Sustainable Energy* 5, no. 2 (2013): 023122. <https://doi.org/10.1063/1.4798411>
- [11] Chamoli, Sunil, and N. S. Thakur. "Correlations for solar air heater duct with V-shaped perforated baffles as roughness elements on absorber plate." *International Journal of Sustainable Energy* 35, no. 1 (2016): 1-20. <https://doi.org/10.1080/14786451.2013.857318>
- [12] Chamoli, S., and N. S. Thakur. "Exergetic performance evaluation of solar air heater having V-down perforated baffles on the absorber plate." *Journal of Thermal Analysis and Calorimetry* 117, no. 2 (2014): 909-923. <https://doi.org/10.1007/s10973-014-3765-8>
- [13] Karwa, Rajendra, S. C. Solanki, and J. S. Saini. "Heat transfer coefficient and friction factor correlations for the transitional flow regime in rib-roughened rectangular ducts." *International Journal of Heat and Mass Transfer* 42, no. 9 (1999): 1597-1615. [https://doi.org/10.1016/S0017-9310\(98\)00252-X](https://doi.org/10.1016/S0017-9310(98)00252-X)
- [14] Layek, Apurba, J. S. Saini, and S. C. Solanki. "Second law optimization of a solar air heater having chamfered rib-groove roughness on absorber plate." *Renewable Energy* 32, no. 12 (2007): 1967-1980. <https://doi.org/10.1016/j.renene.2006.11.005>
- [15] Yadav, Sanjay, and Maneesh Kaushal. "Nusselt number and friction factor correlations for solar air heater duct having protrusions as roughness elements on absorber plate." *Experimental Thermal and Fluid Science* 44 (2013): 34-41. <https://doi.org/10.1016/j.expthermflusci.2012.05.011>
- [16] Yadav, Sanjay, and Maneesh Kaushal. "Exergetic performance evaluation of solar air heater having arc shape oriented protrusions as roughness element." *Solar Energy* 105 (2014): 181-189. <https://doi.org/10.1016/j.solener.2014.04.001>
- [17] Singh, Sukhmeet, Subhash Chander, and J. S. Saini. "Heat transfer and friction factor correlations of solar air heater ducts artificially roughened with discrete V-down ribs." *Energy* 36, no. 8 (2011): 5053-5064. <https://doi.org/10.1016/j.energy.2011.05.052>
- [18] Singh, Sukhmeet, Subhash Chander, and J. S. Saini. "Exergy based analysis of solar air heater having discrete V-down rib roughness on absorber plate." *Energy* 37, no. 1 (2012): 749-758. <https://doi.org/10.1016/j.energy.2011.09.040>
- [19] Phu, Nguyen Minh, Vo Tuyen, and Tu Thien Ngo. "Augmented heat transfer and friction investigations in solar air heater artificially roughened with metal shavings." *Journal of Mechanical Science and Technology* 33, no. 7 (2019): 3521-3529. <https://doi.org/10.1007/s12206-019-0646-x>
- [20] Phu, Nguyen Minh, Tran The Bao, Hoang Nam Hung, Ngo Thien Tu, and Nguyen Van Hap. "Analytical predictions of exergoeconomic performance of a solar air heater with surface roughness of metal waste." *Journal of Thermal Analysis and Calorimetry* (2020). <https://doi.org/10.1007/s10973-020-09787-5>

- [21] Ngo, Tu Thien, and Nguyen Minh Phu. "Computational fluid dynamics analysis of the heat transfer and pressure drop of solar air heater with conic-curve profile ribs." *Journal of Thermal Analysis and Calorimetry* 139, no. 5 (2020): 3235-3246. <https://doi.org/10.1007/s10973-019-08709-4>
- [22] Phu, Nguyen Minh, and Nguyen Van Hap. "Performance Evaluation of a Solar Air Heater Roughened with Conic-Curve Profile Ribs Based on Efficiencies and Entropy Generation." *Arabian Journal for Science and Engineering* (2020). <https://doi.org/10.1007/s13369-020-04676-3>
- [23] Kottayat, Nidhul, Sachin Kumar, Ajay Kumar Yadav, and S. Anish. "Enhanced thermo-hydraulic performance in a V-ribbed triangular duct solar air heater: CFD and exergy analysis." *Energy* (2020): 117448. <https://doi.org/10.1016/j.energy.2020.117448>
- [24] Saini, S. K., and R. P. Saini. "Development of correlations for Nusselt number and friction factor for solar air heater with roughened duct having arc-shaped wire as artificial roughness." *Solar Energy* 82, no. 12 (2008): 1118-1130. <https://doi.org/10.1016/j.solener.2008.05.010>
- [25] Sahu, Mukesh Kumar, and Radha Krishna Prasad. "Exergy based performance evaluation of solar air heater with arc-shaped wire roughened absorber plate." *Renewable Energy* 96 (2016): 233-243. <https://doi.org/10.1016/j.renene.2016.04.083>
- [26] Phila, A., S. Eiamsa-ard, and C. Thianpong. "Thermal performance evaluation of a channel installed with inclined-baffle turbulators." *Arabian Journal for Science and Engineering* 45, no. 2 (2020): 609-621. <https://doi.org/10.1007/s13369-019-04097-x>
- [27] Luan, Nguyen Thanh, and Nguyen Minh Phu. "Thermohydraulic correlations and exergy analysis of a solar air heater duct with inclined baffles." *Case Studies in Thermal Engineering* (2020): 100672. <https://doi.org/10.1016/j.csite.2020.100672>
- [28] Phu, Nguyen Minh, and Geun Sik Lee. "Characteristics of pressure and force considering friction in a closed cylinder with a holed piston." *Journal of Mechanical Science and Technology* 28, no. 6 (2014): 2409-2415. <https://doi.org/10.1007/s12206-014-0533-4>
- [29] Phu, Nguyen Minh. "Overall optimization and exergy analysis of an air conditioning system using a series-series counterflow arrangement of water chillers." *International Journal of Air-Conditioning and Refrigeration* 27, no. 04 (2019): 1950034. <https://doi.org/10.1142/S2010132519500342>
- [30] Altfeld, K., W. Leiner, and M. Fiebig. "Second law optimization of flat-plate solar air heaters Part I: The concept of net exergy flow and the modeling of solar air heaters." *Solar Energy* 41, no. 2 (1988): 127-132. [https://doi.org/10.1016/0038-092X\(88\)90128-4](https://doi.org/10.1016/0038-092X(88)90128-4)
- [31] Ghritlahre, Harish K., and Radha K. Prasad. "Prediction of exergetic efficiency of arc shaped wire roughened solar air heater using ANN model." *International Journal of Heat and Technology* 36, no. 3 (2018): 1107-1115. <https://doi.org/10.18280/ijht.360343>
- [32] Ghritlahre, Harish Kumar. "Development of feed-forward back-propagation neural model to predict the energy and exergy analysis of solar air heater." *Trends in Renewable Energy* 4, no. 2 (2018): 213-235. <https://doi.org/10.17737/tre.2018.4.2.0078>
- [33] Ghritlahre, Harish Kumar, and Radha Krishna Prasad. "Exergetic performance prediction of solar air heater using MLP, GRNN and RBF models of artificial neural network technique." *Journal of Environmental Management* 223 (2018): 566-575. <https://doi.org/10.1016/j.jenvman.2018.06.033>
- [34] Ghritlahre, Harish Kumar, and Radha Krishna Prasad. "Exergetic performance prediction of a roughened solar air heater using artificial neural network." *Strojniški vestnik-Journal of Mechanical Engineering* 64, no. 3 (2018): 194-206. <https://doi.org/10.5545/sv-jme.2017.4575>